FAST RAY TRACING OF LUNAR DIGITAL ELEVATION MODELS. T. P. McClanahan[1] (timothy.p.mcclanahan@nasa.gov), L.G. Evans[2], R.D. Starr[3], I. Mitrofanov[4], [1]NASA Goddard Space Flight Center, Building 2 Room 129, Greenbelt, MD 20771. [2]Computer Sciences Corp. at NASA/GSFC [3]Catholic University at NASA/GSFC [4]Institute for Space Research, Moscow, Russia

Introduction: Ray-tracing (RT) of Lunar Digital Elevation Models (DEM)'s is performed to virtually derive the degree of radiation incident to terrain as a function of time, orbital and ephemeris constraints [1-4]. This process is an integral modeling process in lunar polar research and exploration due to the present paucity of terrain information at the poles and mission planning activities for the anticipated spring 2009 launch of the Lunar Reconnaissance Orbiter (LRO). As part of the Lunar Exploration Neutron Detector (LEND) and Lunar Crater Observation and Sensing Satellite (LCROSS) preparations RT methods are used to estimate the critical conditions presented by the combined effects of high latitude, terrain and the moons low obliquity [5-7]. These factors yield low incident solar illumination and subsequently extreme thermal, and radiation conditions.

The presented research uses RT methods both for radiation transport modeling in space and regolith related research as well as to derive permanently shadowed regions (PSR)'s in high latitude topographic minima, e.g craters. These regions are of scientific and human exploration interest due to the near constant low temperatures in PSR's, inferred to be < 100° K. Hydrogen is thought to have accumulated in PSR's through the combined effects of periodic cometary bombardment and/or solar wind processes, and the extreme cold which minimizes hydrogen sublimation [8-9]. RT methods are also of use in surface position optimization for future illumination dependent on-surface resources e.g. power and communications equipment [10-11].

However, ray-tracing methods are computationally slow due to the inherent vector transport process and the subsequent search phase required to evaluate, identify, and interact with surfaces [12]. The issue is exacerbated if the DEM point surface is converted to a plate model due to the large number of floating point operations (48) required to evaluate each plate facet [13-14]. As a result, the computational complexity incurred in evaluating direct illumination without optimization constraints increases exponentially as a function of the product of the number of surfaces n in the model evaluated against all other surfaces during search $s \sim |\boldsymbol{n}|-1$, floating point operations per surface evaluation f, number of vectors projected per pixel $|v|$, $O(nsfv)$. In this case, the exponential time-complexity increases effectively limit the scale or resolution of the model size $|n|$. In this research, we effectively minimize the search space size $|s|$ and floating point operations $|f|$, by using vector-point operations, *thereby significantly improving the algorithm run-time.*

Methods: Significant computational performance gains are obtained by not triangulating the DEM surface points into plates. Instead, vector-point operations facilitate fast evaluation for direct illumination and secondary illumination processes, lines (1-9). In this approach **DEM** surface points are warped to a sphere (Moon 1734.8 km radius) illustrated in *Figure 1*. Given point $\mathbf{p}_i$ as an arbitrary pixel in image **DEM** for which illumination conditions are required, each point must be evaluated for the possibility of shading. The Sun is oriented at Cartesian position **sun**. $\mathbf{v}_i$ defines the vector between the **sun** and $\mathbf{p}_i$ (1). **sun** to $\mathbf{p}_i$ distance = $dist_i$ (2). (3) normalizes $\mathbf{v}_i$. (4) defines a linear set $\mathbf{dv}_i$ of distance scalars from **sun** as interpolants along $\mathbf{v}_i$ at interval, α (km). $\mathbf{dv}_i$ range = [$dist_i$ - *range*, $dist_i$]. $|\mathbf{dv}_i| = range / \alpha$. (5) A discrete set of Cartesian positions **pos** ε $\mathbf{v}_i$ are determined by projecting from **sun** along $\mathbf{v}_i$ at distances defined by set $\mathbf{dv}_i$. (6) *npos* defines the number of positions in **pos** to be evaluated for shading of $\mathbf{p}_i$. (7-11) evaluates each point in **pos** as to its elevation by rounding its (x,y) coordinates to common coordinates that index the elevation scalar in **v** and **DEM**. In conditions where the elevation z value in the DEM is higher than the z value in v, a 'shade' condition is identified.

These steps provide a nearly direct access methodology that significantly minimizes the search space for evaluating illumination for each $\mathbf{p}_i$, evaluating only possible occluding positions along vector, $\mathbf{v}_i$. Starting evaluation of **pos** at $dist_i$, and working towards the sun along $\mathbf{v}_i$, facilitates a run time minimization of searching $\mathbf{dv}_i$ by monitoring local elevation conditions and shaded status to terminate the loop. A consequence of this approach is that actual intersection points of $\mathbf{v}_i$ with the surface are not determined. These may be approximated using interpolation with **sun** distances to nearest neighbor points.

Secondary vector projection processes require surface intersection points and surface normal information. A given vector-surface intersection point $\mathbf{pos}_i$ is obtained by proceeding through each element in **pos** starting at $\mathbf{p}_i$ to determine the closest shading point $\mathbf{p}_n$. Surface normals at each point are pre-calculated for

each model by taking the vector cross product between adjacent points. These are averaged to yield DEM normals for each point.

```
1.    v_i = p_i − sun
2.    dist_i = |v_i|
3.    v_i = v_i / dist_i
4.    dv_i = interpol(dist_i, range, α)
5.    pos = sun + v*dv_i
6.    npos = range/α
7.    for j = 1, npos do
8.       x = round(pos(0,j))
9.       y = round(pos(1,j))
10.      if DEM(x,y) gt pos(2,j) then
                'Shade
11.   endfor
```

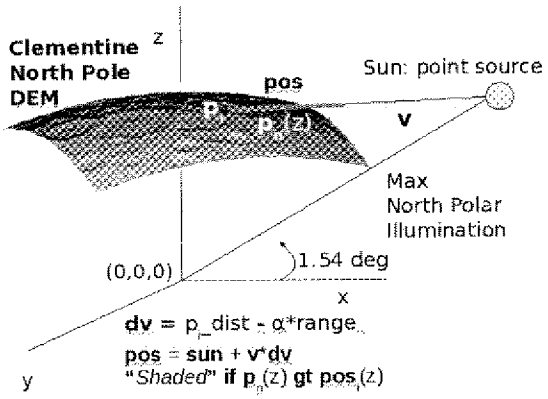

Figure 1. Example of single vector direct solar illumination. Illumination process is optimized by minimizing the number of floating point operations for surface evaluations as well as the ray-tracing search space. Multiple vector projections are also supported

Results: *Figure 2* illustrates both permanently shadowed and illuminated regions of the Clementine North Polar DEM containing 80-90 deg north latitude [15-16]. Image resolution (606x606) pixels = 1km^2/ pixel during summer where the north pole is inclined 1.54° towards the sun, yielding maximum north polar illumination. In this approach, the sun position was rotated in 1° increments around the DEM for 360 degrees yielding 360 images. Without further optimization, each point's direct illumination is evaluated against all points n for shading incurring $|n|^2$ = 367236 evaluations to determine the maps direct shading for each image. Only α spaced points along the incident solar vector **v** are evaluated with maximum required search map corner to corner *range* = 808 points. By integrating through the image stack in each pixel, degree of illumination is determined. Highlighted PSR's generally occur in the bottoms of craters below the southern rim, area=1661 km^2 (*red*). *Note*: linear and blocky structures in the DEM are false positives incurred by elevation mis-registrations in the overlay of the Clementine source imagery during DEM formulation. Updates to these products will increase the resolution and accuracy of DEM's, modifying the stated PSR and illuminated areas.

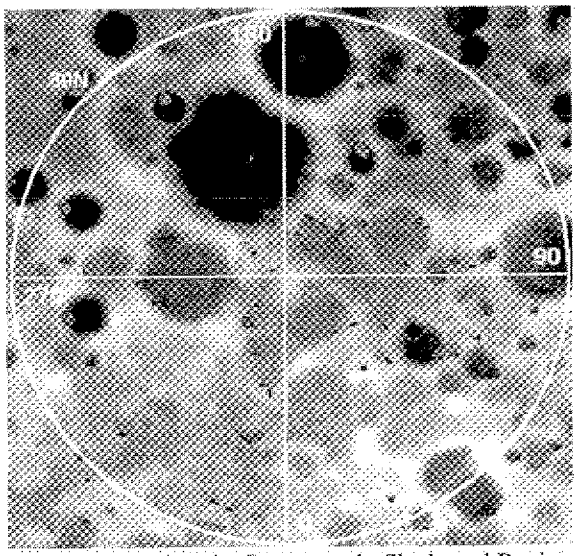

Figure 2. North Polar Permanently Shadowed Regions derived from Clementine DEM using ray-tracing methods for 360, 1° rotation increments during North Polar summer when polar inclination = 1.54°, yielding maximum illumination. Demonstration used the described enhanced ray-tracing methods to derive illumination.

References:

[1] Blewett T.B. LEAG-ICEUM-SSR, (2008) [2] Slade M. A. *Lun Crat Obs and Sens. Sat Site Sel.*, [3] Matsushima T. *Earth and Space 2006, Const. and Eng. in Chall. Env.* (2006) [4] Margot J.L. et. al. *Science*, 284:1658-1660 (1999) [5] Garrick-Bethell I. et. al. LPSC XXXVI, (2005) [6] Chin G. LPSC XXXVII (2006) [7] Chin G. Space Sci. Rev. 129:391-419 (2007) [8] Arnold J. JGR, 84:5659-5668 (1979) [9] Crider D.H. *JGR* 108(E7)(2002) [10] Fincannon H.J. 6th Int. Energy Conv. and Eng. Conf., (2008) [11] Fincannon H.J. *46th AIAA Aero. Sci. Meet. and Exhib* (2008) [12] Hurley J. *Intel Tech Journ.* 9(02) (2005) [13] Badouel D. *Graphics Gems* (1990) [14] O'Rourke *Comp. Geom. in C* (1997) [15] Nozette S. et. al. *Science* (1994) [16] Rosiek M.R. LPSC XXXVIII (2007) [17] Mitrofanov I. *Astrobiology* (2008)